POLITECNICO DI TORINO
Repository ISTITUZIONALE

Systematic Monte Carlo Analysis of Binary Compounds for Neutron Shielding in a Compact Nuclear Fusion Reactor

Original
Systematic Monte Carlo Analysis of Binary Compounds for Neutron Shielding in a Compact Nuclear Fusion Reactor / Calzavara, F., Di Eugenio, N., Ledda, F., Torsello, D., Trotta, A., Gallo, E., Laviano, F.. - In: APPLIED SCIENCES. - ISSN 2076-3417. - ELETTRONICO. - 15:21(2025), pp. 1-13. [10.3390/app152111557]

Availability:
This version is available at: 11583/3004729 since: 2025-11-02T14:01:00Z

Publisher:
MDPI

Published
DOI:10.3390/app152111557

Terms of use:

This article is made available under terms and conditions as specified in the corresponding bibliographic description in the repository

Publisher copyright
AIP postprint versione editoriale con licenza CC BY/Version of Record with CC BY license

Copyright 2025 Author(s). This article is distributed under a Creative Commons Attribution (CC BY) License https://creativecommons.org/licenses/by/4.0/."

(Article begins on next page)

26 November 2026

applied sciences

MDPI

Article

Systematic Monte Carlo Analysis of Binary Compounds for Neutron Shielding in a Compact Nuclear Fusion Reactor

Fabio Calzavara [1,2,†], Niccolò Di Eugenio [1,2,†], Federico Ledda [1,2], Daniele Torsello [1,2], Antonio Trotta [3], Erik Gallo [4] and Francesco Laviano [1,2,*]

[1] Department of Applied Science and Technology, Politecnico di Torino, I-10129 Torino, Italy; fabio.calzavara@polito.it (F.C.); niccolo.dieugenio@polito.it (N.D.E.); federico.ledda@polito.it (F.L.); daniele.torsello@polito.it (D.T.)
[2] Istituto Nazionale di Fisica Nucleare, Sezione di Torino, I-10125 Torino, Italy
[3] Eni S.p.A., MAFE, I-30175 Venice, Italy; antonio.trotta@eni.com
[4] Eni S.p.A., Piazzale Enrico Mattei, 1, I-00144 Roma, Italy; erik.gallo@eni.com
* Correspondence: francesco.laviano@polito.it
† These authors contributed equally to this work.

Abstract

Compact fusion reactors are receiving increasing interest as a promising route for accelerating the path toward commercial fusion, thanks to their reduced size and cost. However, this compactness introduces new technological challenges, including higher radiation loads on critical functional components, such as the magnet system. Neutron shielding is therefore of utmost importance to guarantee the expected lifetime of the device, and its selection must account for the harsh environment imposed by the high radiation flux. Shielding materials should be structurally stable, not melt within the operational temperature windows, and be relatively low-cost. For nuclear reactor applications, binary compounds are typically the preferred choice as they often meet these requirements, particularly in terms of availability and cost. In this work, we present a systematic Monte Carlo analysis of more than 700 binary compounds, exposed to the neutron spectrum at the most loaded position of the vacuum vessel in a simplified model of a compact fusion reactor. Shielding performances were evaluated in a toroidal geometry in terms of neutron attenuation, power deposition, and activation, leading to the identification of several promising compositions for effective neutron shielding in future fusion applications.

Keywords: neutron shielding materials; compact fusion reactors; Monte Carlo simulations

check for updates

Academic Editors: Rongjie Song, Andrea M. Jokisaari and Lingfeng He

Received: 29 September 2025
Revised: 20 October 2025
Accepted: 22 October 2025
Published: 29 October 2025

Citation: Calzavara, F.; Di Eugenio, N.; Ledda, F.; Torsello, D.; Trotta, A.; Gallo, E.; Laviano, F. Systematic Monte Carlo Analysis of Binary Compounds for Neutron Shielding in a Compact Nuclear Fusion Reactor. *Appl. Sci.* **2025**, *15*, 11557. https://doi.org/10.3390/app152111557

Copyright: © 2025 by the authors. Licensee MDPI, Basel, Switzerland. This article is an open access article distributed under the terms and conditions of the Creative Commons Attribution (CC BY) license (https://creativecommons.org/licenses/by/4.0/).

1. Introduction

The recent commercial availability of high-temperature superconductors, capable of sustaining significantly higher magnetic fields, has marked a breakthrough in fusion research, enabling a reduction in the size of conventional tokamaks and, consequently, in the cost of the first demonstrators [1]. The possibility of designing fusion-relevant devices without the budget of large collaborations or massive public projects has made this approach highly appealing, attracting considerable attention and funding from both private and public institutions [2]. However, the strong reduction in size introduces new challenges for these fusion machines, among which radiation damage to the magnet system is particularly critical [3–5]. The most promising fusion reaction, deuterium–tritium (D-T), produces 14 MeV neutrons that escape the plasma and transport energy through the reactor structures. Due to their neutral nature, neutrons undergo relatively few interactions

while passing through materials, which allows them to travel long distances and easily reach even remote and delicate components such as the magnets [6]. In compact reactors, where the space between the plasma and the magnets is strongly reduced, this effect becomes particularly critical. Several recent studies have highlighted the alarmingly high particle fluxes and radiation damage expected in the magnets of compact reactors (see, for example, [7]), and the computational study of effective neutron shielding has been identified as a key milestone in the fusion roadmap by the scientific community [8].

The choice of the shielding material for protecting the components of the machine must be made carefully, taking into account the harsh environment to which it will be exposed, as well as technological and engineering constraints. The material should ensure good radiation attenuation, be structurally stable, remain solid within the operating temperature windows, and be relatively low-cost. Binary compounds are generally used for this purpose in the nuclear industry, as they often meet these requirements [9–11]. They can synergistically combine favorable nuclear properties by pairing an element with a high neutron capture or reflection cross-section, such as boron or tungsten, with another element that effectively thermalizes neutrons or provides a mechanically stable matrix, such as hydrogen or carbon. In addition, many of these compounds exhibit high chemical and thermal stability and high melting points, and can be engineered in various forms, such as composites or ceramics.

In this context, we present a large-scale study of the shielding properties of 718 binary compounds, combining composition and density data from the Materials Project database [12] with Monte Carlo (MC) transport and activation simulations. Numerical approaches of this kind have been widely adopted over recent decades owing to continual improvements in computational performance, and they have proven useful in a variety of applications [13–15]. The effects of the neutron flux going out from the most loaded position of the vacuum vessel of a compact fusion machine (e.g., an ARC-like reactor [16]) were simulated using a simplified tokamak-like geometry, consisting of a toroidal shell based on the dimensions proposed in [1]. This allowed for the evaluation of neutron attenuation through the shielding material, as well as several key parameters for characterizing material behavior, such as Power Density Deposition (PDD). Moreover, a comparative analysis of the results is carried out, enabling us to suggest the most promising candidates for experimental testing. This multi-simulation approach is designed to generate a large dataset for future research on the shielding properties of materials under neutron irradiation, paving the ground for AI-based methods. Although the work is primarily focused on fusion applications, the methods described here can be easily generalized to a wide range of contexts, making the results potentially useful across various scientific fields.

2. Materials and Methods

In this section, we provide an overview of the data source used for our simulations and highlight the key aspects of the analysis, in order to clarify the starting point of the following discussion.

2.1. Materials Data

To compile the dataset needed for this study, a brute-force querying approach was employed, through the use of the Materials Project API (mp-api) [17]. Specifically, a custom Python v.3.12 script that employs the mp-api and pymatgen [18] libraries was conceived. Such a script iteratively queries the database, looking for stable binary compounds containing one period-two target element (from the first and second rows the periodic table without noble gases), chosen because of their light atomic mass. Additional filtering was applied to each material in order to consider only compounds containing elements with an

atomic number less than or equal to 92. The resulting dataset, in the form of the simplified chemical composition, density, and atomic numbers of the constituent elements, was then employed to create the input files of the MC simulations. This brute-force approach thus ensures a fast and complete extraction of eligible materials, which makes it versatile for application in other contexts and processes.

2.2. Monte Carlo and Activation Simulations

In the present work, MC simulations were performed employing the Particle and Heavy Ion Transport code System (PHITS) [19] (version 3.341) and its native nuclear data library Japanese Evaluated Nuclear Data Library (JENDL-4.0) [20]. PHITS is a multiplatform, multipurpose FORTRAN-based MC code and is developed by the Japanese Atomic Energy Agency (JAEA). The code has been compared to other widely used MC codes, like OpenMC, and has already been applied for radiation damage modeling on superconducting magnets [16,21].

The model geometries, representing the shield of an ARC-like reactor, were defined directly in PHITS using its native Constructive Solid Geometry (CSG) framework. A simplified toroidal shell was built with a major radius of 300 cm, an inner minor radius of 110 cm, and a thickness of 20 cm. The total shield volume is approximately 3.1 m^3. This simplified model was adopted to propose an automated workflow and reduce computational time. Each simulation had a statistic of 1×10^7 particles, divided into 47 batches (2.1×10^5 particles per batch). The neutron spectrum outgoing from the most loaded position of the vacuum vessel of an ARC-like reactor, reported in [16], is presented in Figure 1b. An isotropic ring source of radius 300 cm, located inside the torus, as shown in Figure 1a, was set so that this neutron spectrum and flux impinged on the shield in our simulations. The transmitted and reflected fluxes of various particles (neutrons, photons, electrons, and protons) were evaluated using a regional mesh in the T-TRACK tally, employing two fictitious 1 mm thick shells placed near the inner and outer surfaces of the main torus, to evaluate both the integral and spectral shielding performances of the selected materials. In addition, we evaluate PDD within the material, with the aim of generating a rich dataset that enables the identification of potentially useful correlations and previously unexplored phenomena.

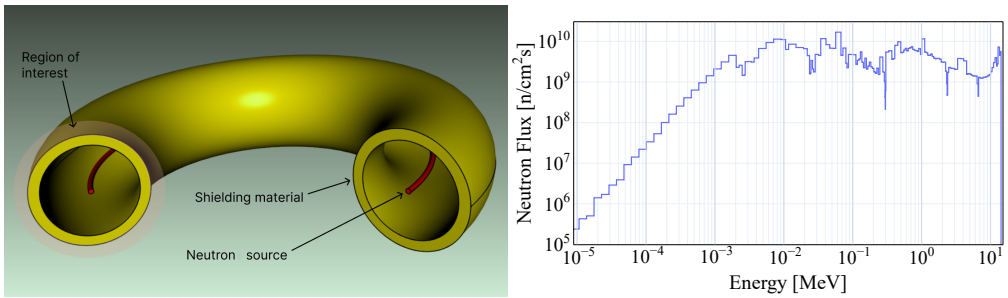

(**a**) (**b**)

Figure 1. Two main inputs of the analysis are shown. (**a**) Cross-section of the simplified geometry used in the MC simulations. (**b**) Neutron flux spectrum implemented as the irradiation source.

After thoroughly analyzing the entire dataset, a small subset of compounds was selected for detailed activation analysis using the DCHAIN code [22]. DCHAIN is a decay chain analysis tool that simulates the time-dependent decay of nuclides in a given radiation environment. It is natively coupled with PHITS, which can automatically generate the input files required for the activation calculations. Both maintenance and end-of-life scenarios were simulated: the former considers two 1-year periods of burning plasma separated by

a 2-month shutdown, while the latter evaluates the decay after 10 full-power years (FPY) of operation.

3. Results

In this section, we present the results of the MC simulations and the subsequent analysis that leads to the selection of a series of best candidates for neutron shielding applications.

3.1. Full Dataset Results

In order to quantify the shielding performance of the selected materials in terms of neutron flux attenuation, which represents the primary focus of the analysis, it is useful to introduce a parameter defined as the ratio between the neutron flux density incident on the shield (integrated over the full energy range employed and expressed in n cm^{-2} s^{-1}), and the same quantity emerging outside of it. This parameter will be referred to as the Neutron Flux Ratio (NFR). A comprehensive overview of the results obtained from the entire dataset is shown in Figure 2, where the NFR is plotted as a function of PDD.

The horizontal dotted line, corresponding to NFR = 0.802, denotes the reference case (i.e., the absence of shielding material) and highlights the flux density reduction attributable to purely geometrical effects. In that case, although the total number of neutrons is conserved, they are spread over a larger exit surface area; consequently, the void reference value differs from 1. Thus, a value of 0 denotes perfect shielding, while NFR = 0.802 corresponds to no shielding: the outgoing flux equals the incoming flux, and the material does not contribute to the flux density decrease. Moreover, materials above this line increase the neutron flux relative to the void case due to neutron multiplication driven by their nuclear cross-sections. As an example, BeO exhibits an NFR of 0.93; this neutron enhancement mainly results from the (n, 2n) and (γ, n+2α) reaction channels. Another interesting observation from the figure is that most of the data present a linear dependence of NFR on PDD. This behavior is readily explained: a lower NFR corresponds to a stronger neutron interaction, and therefore (if the interaction is inelastic) to a larger amount of power deposited in the material.

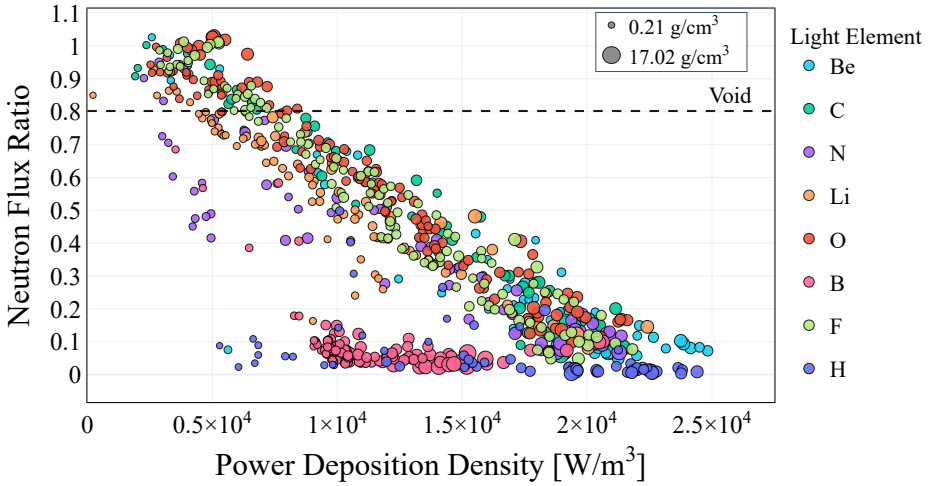

Figure 2. NFR as a function of PDD for the full set of materials. Dot size corresponds to the compound density, while color indicates the specific light element present in each compound.

Two main subsets of materials with the most favorable shielding properties can be identified—hydrides and borides—as they ensure a flux ratio below 4%. A more detailed analysis of these two classes will be discussed in the following subsections.

Given the large size of the dataset, several approaches are able to represent the relationships among its key properties. For example, in Figure 3, the NFR is plotted against the

compound density, with a color map indicating the PDD. Higher PDD values are generally associated with improved shielding performance, as the energy of the captured neutrons is deposited in the material.

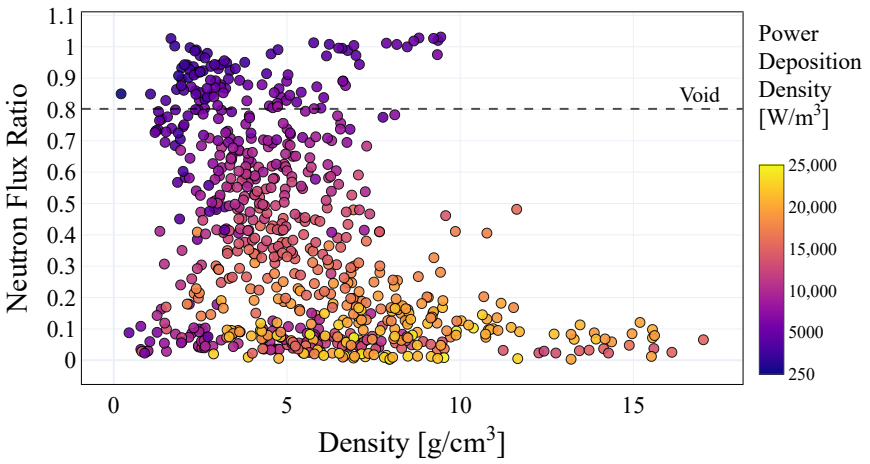

Figure 3. NFR as a function of the density of the compounds, for the full set of materials. Dot color indicates the PDD.

At the same time, PDD is a technologically relevant parameter, as it impacts the design of the cooling system and defines the operational temperature window of the shield. It is noteworthy that materials exhibiting high shielding performance, particularly those belonging to the two most promising classes, hydrides and borides, span a wide range of density values. This suggests that density alone is not a sufficient predictor of shielding effectiveness. Indeed, while higher material density tends to increase the probability of neutron interactions, by effectively scaling the microscopic cross-section through the nuclear number density, the nuclear properties are ultimately governed by the microscopic cross-sections and the elemental composition of the material.

In a further analysis, shown in Figure 4, the NFR is plotted as a function of the atomic number of the heavier element in the compound. The behavior observed in this plot indicates that there is no straightforward correlation between shielding effectiveness and the atomic number of the heavier element, rather highlighting the importance of other specific nuclear properties, such as the nuclear configuration of the element. In this sense, we can observe peaks of low neutron absorption that can be attributed to the enhanced nuclear stability (e.g., nuclei whose neutron numbers are close to magic numbers [23]). While they may not capture neutrons that have been slowed by the light element, they can be fragmented or induced to undergo (n, 2n) reactions by incident neutrons with energies of several MeV or higher. This mechanism could explain why this multiplication is observed.

Indeed, a first insight into what the best candidates should be can be inferred from Figure 5. In this figure, the shielding capabilities are related to the ratio between the total mass of the heavier and the lighter elements in the compound, namely considering the stoichiometry. From the plot, it is clear that the lowest flux ratio is associated with the hydrogen-based component with a medium-high total mass ratio.

Given that most hydrides show the lowest NFR values while borides combine relatively high shielding capability with low PDD values, the following in-depth analysis will be restricted to these two subsets. This choice is also motivated by their widespread use in nuclear applications: hydrides give the best NFR values, whereas borides are widely used as control materials and are a valid alternative if one wants to avoid hydrogen-rich materials in nuclear facilities.

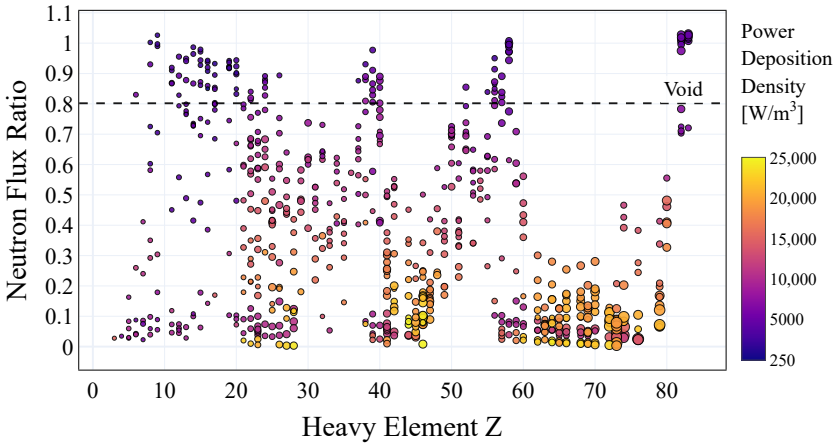

Figure 4. NFR as a function of the atomic number Z of the heavier element in the compound, for the full set of materials. Dot color indicates the PDD.

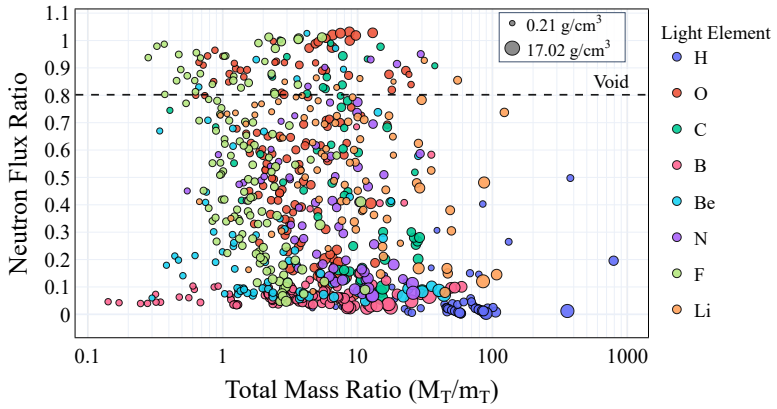

Figure 5. NFR as a function of the material's total mass ratio, for the entire dataset. Marker size represents material density, while color indicates the light element present.

3.2. Borides and Hydrides

Further investigation regarding the properties and performance of both borides and hydrides is thus presented in this subsection. To begin, one of the major aspects to take into account is the availability of materials [24]. In Figure 6, the materials able to provide an NFR smaller than 3.5% are plotted with respect to PDD values, with markers scaled according to the abundance (in the Earth's crust and in the sea) of the heavy element they represent. In this subset, one can find nine compounds, composed mainly of rare elements, with the exception of manganese tetraboride (MnB_4). Despite its high flux ratio with respect to the subset, this compound shows the lowest energy deposition value of the entire set of best candidates.

Another key requirement for nuclear materials is a sufficiently high fusion temperature so that they remain solid under operating conditions. For the purpose of this study, only materials with a melting temperature above 1000 K were selected, employing Materials Project's melting point data, obtained with a graph neural network model [25]. Thermal issues can also arise from gamma-ray production. Large emissions of this radiation can cause severe overheating of nearby components (potentially critical on the magnet system near the shielding layer, which needs to be kept at 20 K or below), while also posing safety issues for the personnel and complications in remote maintenance. For these reasons, it is desirable to investigate and minimize such emissions [26]. In Figure 7, we plot gamma-ray flux—defined here as photons with an energy greater than 10^4 eV—for the best borides, in terms of PDD, with a color map indicating melting temperatures. It is worth noting that the gamma-ray flux decreases exponentially with increasing density of the compound,

as confirmed by our results; however, a detailed analysis of the influence of material density on gamma attenuation is beyond the scope of the present study.

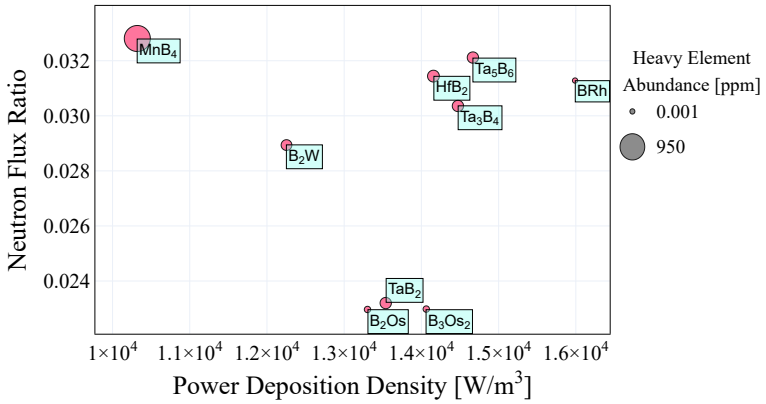

Figure 6. A focus on the most effective borides, with NFR plotted against PDD. The marker size reflects the relative abundance of the associated heavy element.

Within this subset, MnB_4 and BRh show comparatively elevated gamma-ray flux. In the case of MnB_4, the effect is attributable to the $^{55}Mn(n, \gamma)-^{56}Mn$ reaction, frequently exploited for neutron-flux monitoring in nuclear reactors [27,28], which produces gamma radiation.

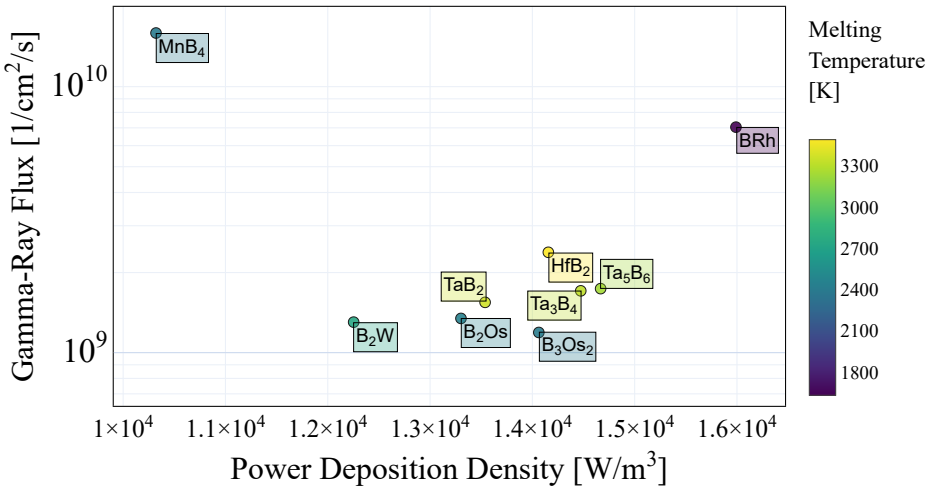

Figure 7. Detailed view of the top-performing borides, showing PDD as a function of gamma-ray flux. Marker color indicates the relative fusion temperature of the compound.

The same plots reported in Figures 6 and 7 are represented for the hydride subset in Figures 8 and 9. These compounds are the best-performing ones in the dataset for neutron shielding applications since they possess the lowest flux ratio values. However, their energy deposition is greater than the values computed for borides. In this subset, TaH_2 exhibits the best shielding performance across the entire dataset, despite the low abundance of Ta (2.00 ppm). Conversely, TiH_2 shows an NFR three times higher than that of TaH_2, but it is the most readily available material within the hydride subset, with titanium's abundance being three orders of magnitude greater than that of tantalum.

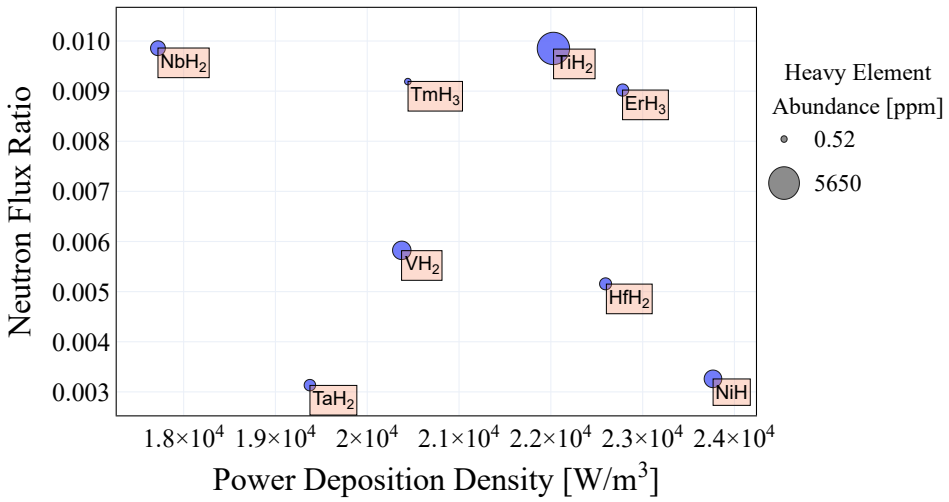

Figure 8. Detailed view of the most effective hydrides, showing NFR versus PDD. Marker size indicates the relative abundance of the corresponding heavy element.

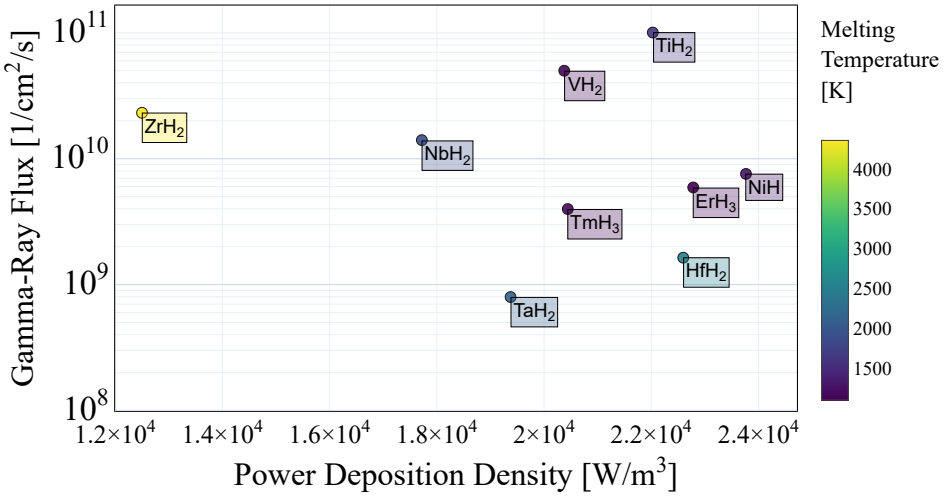

Figure 9. Close-up of the best-performing hydrides, with PDD plotted against gamma-ray flux. Marker color represents the relative fusion temperature of each compound.

4. Discussion

In order to select a set of best candidates, starting from the compounds in the previous section, further analysis was performed, with some considerations:

- ZrH_2 was added as it is widely used in fusion applications and zirconium has higher abundance with respect to other heavy elements [29–31].
- Despite their poorer shielding performance, borides generally exhibit lower levels of PDD and can be preferable in some neutron control applications, as mentioned before. For these reasons, they are included in the set to offer a wider range of options.
- Elements with very low natural abundance are excluded for economic reasons.
- Materials available only under extreme, laboratory-level conditions are not considered.

Thus, the final group is composed of eight compounds: TaH_2, VH_2, HfH_2, TiH_2, ZrH_2, TaB_2, WB_2, and MnB_4. In Table 1, an overview of these materials is presented, showing the following: density values (ρ) and Fusion Temperature (FT) from Materials Project's database; gamma-ray flux (γF), NFR, and PDD from MC simulations; and heavy elements' abundance (HA) from [24].

Table 1. Summary of the top candidate materials for neutron shielding, including key performance metrics such as NFR, PDD, and gamma-ray flux. These entries represent the most effective materials identified from our dataset and were selected based not only on absolute performance but also on additional criteria outlined previously (e.g., relevance to nuclear environments).

Composition	ρ [g/cm^3]	NFR	PDD [W/m^3]	FT [K]	HA [ppm]	γF [1/cm^2 s]
ZrH_2	5.64	0.0248	1.25×10^4	1910	165	2.32×10^{10}
TaH_2	13.20	0.0031	1.94×10^4	2125	2.00	7.97×10^8
VH_2	4.76	0.0058	2.04×10^4	1150	120	5.00×10^9
HfH_2	11.66	0.0051	2.26×10^4	2487	3.00	1.64×10^9
TiH_2	3.88	0.0099	2.20×10^4	1591	5650	1.01×10^{11}
TaB_2	12.27	0.0232	1.35×10^4	3360	2.00	1.55×10^9
WB_2	12.42	0.0289	1.23×10^4	2738	1.25	1.30×10^9
MnB_4	4.53	0.0328	1.03×10^4	2401	950	1.59×10^{10}

For the selected compounds, we performed an in-depth study of neutron attenuation across the entire emission spectrum. As expected, materials within the same subset (hydrides and borides) exhibit very similar behavior. In Figure 10a,b, it can be seen that boron-based materials are more effective at capturing epithermal and resonance neutrons, whereas hydrides tend to produce neutron multiplication in that energy range. The major difference, however, is in the most populated ranges of intermediate energy and fast neutrons: here, the presence of hydrogen causes a heavy decrease in the outward flux, by a factor of between two or three orders of magnitude, while for the borides, it remains between 10^{-2} and 10^{-1}. Overall, this indicates the better shielding performance of hydrides.

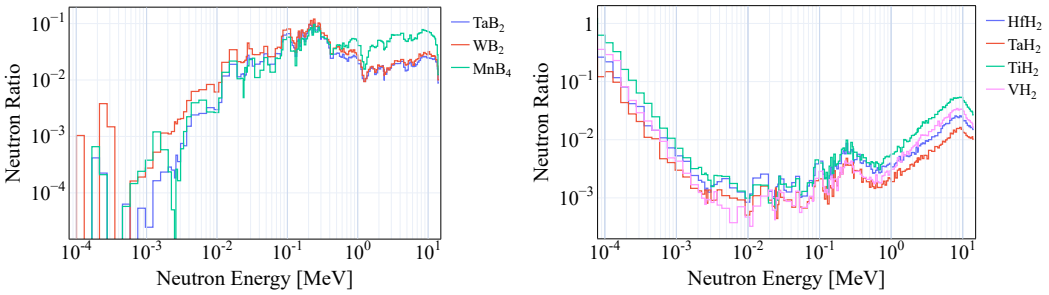

(**a**) Borides (**b**) Hydrides

Figure 10. Attenuation of neutron flux over the energy spectrum for selected boride compounds (on the left) and hydrides (on the right).

A final point concerns the activation of materials exposed to high neutron fluence. Material activation is a crucial factor for worker protection, a reduction in radioactive-waste hazards, and the prevention of damage to reactor components [32]. Activation levels were calculated for each of the compounds shown in Table 1. The resulting activity is plotted as a function of irradiation time in Figure 11 for the entire group of the best candidates, while a focus on borides and hydrides is shown in Figure 12a and Figure 12b, respectively. One can thus observe that the variation in activity levels between the peak reached during irradiation and the lowest values in the shutdown phase is less than one order of magnitude for all compounds, apart from VH_2, which shows both the highest activity values during irradiation and the lowest ones during shutdown, with a decrease of almost five orders of magnitude. On the other hand, TiH_2 has the second-lowest activity value during shutdown while maintaining relatively low activity levels during irradiation, in the range of 10^{15} Bq.

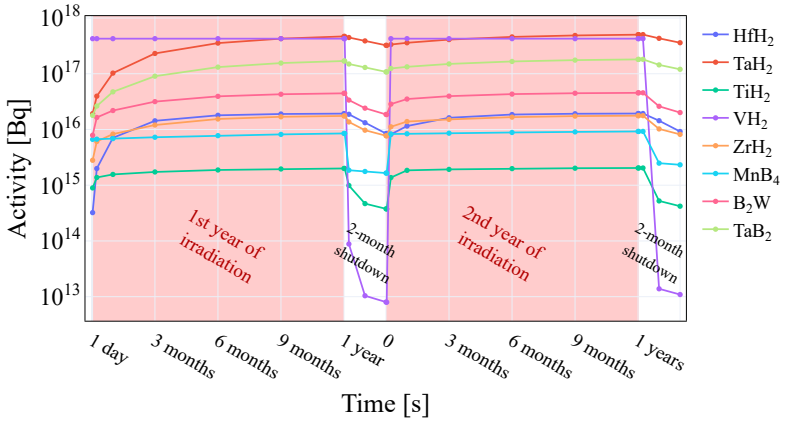

Figure 11. Comparison of simulated activity levels with one year of continuous irradiation at full power, followed by a two-month cooling period.

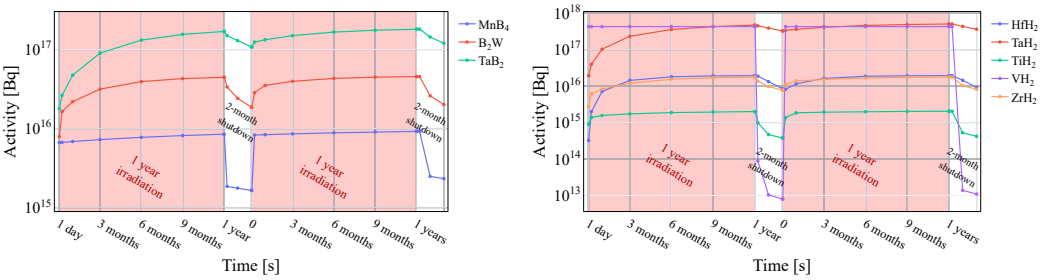

(**a**) Borides (**b**) Hydrides

Figure 12. Activity profiles of selected compounds under a one-year irradiation and two-month shutdown maintenance cycle.

In addition, the end life cycle is shown for both subsets of borides and hydrides in Figure 13, with the two separate plots in Figure 14a,b. The activity levels are shown for a period of 100 years of shutdown, following a precedent ten-year period of full power irradiation.

Once again, VH_2 shows a steep decline as soon as the shutdown period begins; however, its activity levels do not decrease as much as for other hydride compounds, as is the case of TaH_2 and TiH_2, which present the lowest activity values after 100 years, in the range of 10^{-4} Bq. On the other hand, borides show a similar behavior in terms of activity levels' decrease, without however reaching the same values as the hydrides: in fact, the activity is still relatively high (10^{11} Bq) even after 100 years of shutdown.

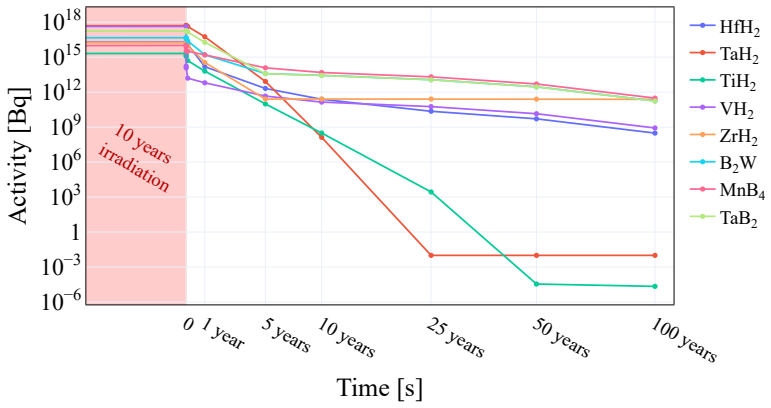

Figure 13. Comparison of predicted activity levels for the best candidate group under end-of-life operating conditions.

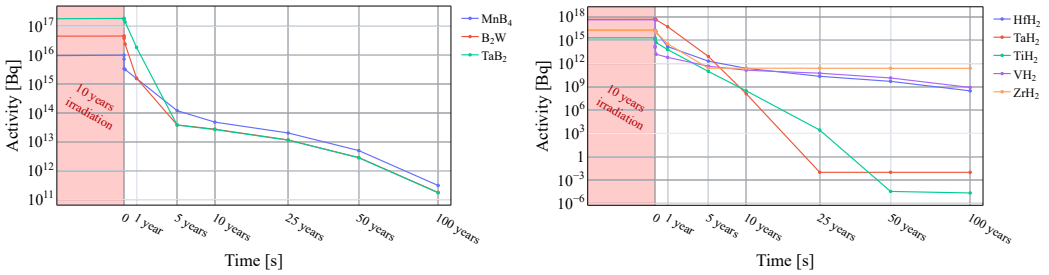

(**a**) Borides (**b**) Hydrides

Figure 14. Predicted activation levels of boride and hydride compounds following end-of-life operational exposure.

Following this comprehensive analysis, considering that it possesses the highest abundance among all best candidates, has a relatively low NFR and, above all, shows low activity values, which are almost negligible after 50 years of shutdown, TiH_2 can be considered the most promising binary compound in this dataset for neutron shielding applications, from a neutronics perspective.

5. Conclusions

In this paper, an automated workflow for inspecting the shielding capability of binary compounds in an ARC-like reactor was shown. MC simulations were performed on simplified tokamak geometries for all compounds extracted from the Materials Project database, in order to extract crucial properties for the characterization of such compounds. Such an approach shows that, in general, hydride and boride compounds possess the lowest NFR values, and for this reason, more detailed analysis was performed only on these two subsets. This further investigation allowed us to select a series of ideal candidates for neutron shielding applications, using the NFR as the driving parameter in the analysis, while also considering other crucial properties like activity levels, availability, and PDD. TiH_2 was individuated as the most promising material for neutron shielding applications, mainly due to the low NFR shown and the almost negligible activity levels during its end-life cycle. This workflow can be extended to the extraction of many more compounds and the computation of crucial physical properties for fusion applications and beyond.

Author Contributions: Conceptualization, D.T. and F.L. (Francesco Laviano); methodology, D.T., F.L. (Federico Ledda) and F.L. (Francesco Laviano); investigation, F.C., N.D.E. and F.L. (Federico Ledda); resources, A.T. and E.G.; data curation, F.C., N.D.E. and F.L. (Federico Ledda); writing—original draft preparation, F.C. and N.D.E.; writing—review and editing, D.T., E.G. and F.L. (Francesco Laviano); visualization, F.C. and N.D.E.; supervision, D.T. and F.L. (Francesco Laviano); project administration, E.G. and F.L. (Francesco Laviano); funding acquisition, E.G., D.T. and F.L. (Francesco Laviano). All authors have read and agreed to the published version of the manuscript.

Funding: This work is partially supported by the Italian Ministry of Foreign Affairs and International Cooperation, grant number US23GR16, and by Eni S.p.A. This work has also been carried out within the framework of the EUROfusion Consortium, funded by the European Union via the Euratom Research and Training Programme (Grant Agreement No 101052200—EUROfusion). The views and opinions expressed are, however, those of the author(s) only and do not necessarily reflect those of the European Union or the European Commission. Neither the European Union nor the European Commission can be held responsible for them.

Institutional Review Board Statement: Not applicable.

Informed Consent Statement: Not applicable.

Data Availability Statement: All data needed to evaluate the conclusions in the paper are included in the manuscript. Additional data related to this paper may be obtained from the corresponding author upon reasonable request.

Acknowledgments: Technical support from CINECA for HPC resources (ENI-HPC4 and Leonardo) is ackowledged.

Conflicts of Interest: Antonio Trotta and Erik Gallo are employed by Eni S.p.A. The remaining authors declare that the research was conducted in the absence of any commercial or financial relationships that could be construed as a potential conflict of interest. The authors declare that this study received funding from Eni S.p.A. The funder was not involved in the study design, collection, analysis, interpretation of data, the writing of this article or the decision to submit it for publication.

References

1. Sorbom, B.; Ball, J.; Palmer, T.; Mangiarotti, F.; Sierchio, J.; Bonoli, P.; Kasten, C.; Sutherland, D.; Barnard, H.; Haakonsen, C.; et al. ARC: A compact, high-field, fusion nuclear science facility and demonstration power plant with demountable magnets. *Fusion Eng. Des.* **2015**, *100*, 378–405. [CrossRef]
2. Meschini, S.; Laviano, F.; Ledda, F.; Pettinari, D.; Testoni, R.; Torsello, D.; Panella, B. Review of commercial nuclear fusion projects. *Front. Energy Res.* **2023**, *11*, 1157394. [CrossRef]
3. Iliffe, W.; Chislett-McDonald, S.; Harden, F.; Adams, K.; Tufnail, J.; Grovenor, C.; Speller, S.; Reilly, A.; Wimbush, S.C.; Nasr, E. Progress in the STEP Programme Toward Understanding REBCO Coated Conductors in the Fusion Environment. *IEEE Trans. Appl. Supercond.* **2025**, *35*, 6602105. [CrossRef]
4. Torsello, D.; Gambino, D.; Gozzelino, L.; Trotta, A.; Laviano, F. Expected radiation environment and damage for YBCO tapes in compact fusion reactors. *Supercond. Sci. Technol.* **2022**, *36*, 014003. [CrossRef]
5. Zhai, Y.; Larbalestier, D.; Duckworth, R.; Hartwig, Z.; Prestemon, S.; Forest, C. R&D Needs for a U.S. Fusion Magnet Base Program. *IEEE Trans. Appl. Supercond.* **2024**, *34*, 4200705. [CrossRef]
6. Bae, J.W.; Peterson, E.; Shimwell, J. ARC reactor neutronics multi-code validation. *Nuclear Fusion* **2022**, *62*, 066016. [CrossRef]
7. Torsello, D.; Ledda, F.; Sparacio, S.; Eugenio, N.D.; Giacomo, M.D.; Gallo, E.; Hartwig, Z.; Trotta, A.; Laviano, F. Radiation Environment and Damage of HTS Magnets in an ARC-Like Reactor. *IEEE Trans. Appl. Supercond.* **2025**, *35*, 4200206. [CrossRef]
8. Torsello, D.; Celentano, G.; Civale, L.; Corato, V.; Eisterer, M.; Gambino, D.; Murphy, S.; Speller, S.; Laviano, F. Roadmap for the investigation of irradiation effects in HTS for fusion. *Supercond. Sci. Technol.* **2025**, *38*, 053501. [CrossRef]
9. Segantin, S.; Meschini, S.; Testoni, R.; Zucchetti, M. Preliminary investigation of neutron shielding compounds for ARC-class tokamaks. *Fusion Eng. Des.* **2022**, *185*, 113335. [CrossRef]
10. Chen, Y.; Yan, B. The technology of shielding design for nuclear reactor: A review. *Prog. Nucl. Energy* **2023**, *161*, 104741. [CrossRef]
11. Chandrasekhar, K.; Lin-Vines, A.; Wilson, C.; Kamal, G.S.; Rajput, M. Shielding Material Performance in a Preconcept Spherical Tokamak Power Plant. *Nucl. Sci. Eng.* **2025**, 1–13. [CrossRef]
12. Jain, A.; Ong, S.P.; Hautier, G.; Chen, W.; Richards, W.D.; Dacek, S.; Cholia, S.; Gunter, D.; Skinner, D.; Ceder, G.; et al. Commentary: The Materials Project: A materials genome approach to accelerating materials innovation. *APL Mater.* **2013**, *1*, 011002. [CrossRef]
13. Attia, M.; Abdalateif, A. Monte Carlo Simulation of Neutrons Scattering in the Reactor. *Int. J. Adv. Sci. Res. Eng.* **2018**, *4*, 51–57. [CrossRef]
14. Blaickner, M.; Demirel, B.; Drevenšek-Olenik, I.; Fally, M.; Flauger, P.; Geltenbort, P.; Hasegawa, Y.; Kurinjimala, R.; Ličen, M.; Pruner, C.; et al. Monte-Carlo simulation of neutron transmission through nanocomposite materials for neutron-optics applications. *Nucl. Instrum. Methods Phys. Res. Sect. A Accel. Spectrometers Detect. Assoc. Equip.* **2019**, *916*, 154–157. [CrossRef]
15. Yang, S.; Yao, Y.; Wang, H.; Huang, H. A Comparative Study of Neutron Shielding Performance in Al-Based Composites Reinforced with Various Boron-Containing Particles for Radiotherapy: A Monte Carlo Simulation. *Nanomaterials* **2024**, *14*, 1696. [CrossRef]
16. Ledda, F.; Pettinari, D.; Ferrero, G.; Hartwig, Z.; Laviano, F.; Meschini, S.; Sparacio, S.; Testoni, R.; Torsello, D.; Trotta, A.; et al. 3D neutronic analysis on compact fusion reactors: PHITS-OpenMC cross-comparison. *Fusion Eng. Des.* **2024**, *202*, 114323. [CrossRef]
17. Ong, S.P.; Cholia, S.; Jain, A.; Brafman, M.; Gunter, D.; Ceder, G.; Persson, K.A. The Materials Application Programming Interface (API): A simple, flexible and efficient API for materials data based on REpresentational State Transfer (REST) principles. *Comput. Mater. Sci.* **2015**, *97*, 209–215. [CrossRef]
18. Ong, S.P.; Richards, W.D.; Jain, A.; Hautier, G.; Kocher, M.; Cholia, S.; Gunter, D.; Chevrier, V.L.; Persson, K.A.; Ceder, G. Python Materials Genomics (pymatgen): A robust, open-source python library for materials analysis. *Comput. Mater. Sci.* **2013**, *68*, 314–319. [CrossRef]

19. Sato, T.; Iwamoto, Y.; Hashimoto, S.; Ogawa, T.; Furuta, T.; Abe, S.I.; Kai, T.; Matsuya, Y.; Matsuda, N.; Hirata, Y.; et al. Recent improvements of the particle and heavy ion transport code system – PHITS version 3.33. *J. Nucl. Sci. Technol.* **2024**, *61*, 127–135. [CrossRef]
20. Shibata, K.; Iwamoto, O.; Nakagawa, T.; Iwamoto, N.; Ichihara, A.; Kunieda, S.; Chiba, S.; Furutaka, K.; Otuka, N.; Ohsawa, T.; et al. JENDL-4.0: A New Library for Nuclear Science and Engineering. *J. Nucl. Sci. Technol.* **2011**, *48*, 1–30. [CrossRef]
21. Ledda, F.; Torsello, D.; Pettinari, D.; Sparacio, S.; Hartwig, Z.; Zucchetti, M.; Laviano, F. 3D Neutronic and Secondary Particles Analysis on $YBa_2Cu_3O_{7-\delta}$ Tapes for Compact Fusion Reactors. *IEEE Trans. Appl. Supercond.* **2024**, *34*, 4206105. [CrossRef]
22. Tasaka, K. *DCHAIN 2: A Computer Code for Calculation of Transmutation of Nuclides*; Technical report; Japan Atomic Energy Research Institute: Tokyo, Japan, 1980.
23. Wigner, E. On the Consequences of the Symmetry of the Nuclear Hamiltonian on the Spectroscopy of Nuclei. *Phys. Rev.* **1937**, *51*, 106–119. [CrossRef]
24. Haynes, W.M. Abundance of Elements in the Earth's Crust and in the Sea. In *CRC Handbook of Chemistry and Physics*, 97th ed.; Chapter Section 14; CRC Press: Boca Raton, FL, USA, 2016; pp. 14–17.
25. Hong, Q.J.; Ushakov, S.V.; van de Walle, A.; Navrotsky, A. Melting temperature prediction using a graph neural network model: From ancient minerals to new materials. *Proc. Natl. Acad. Sci. USA* **2022**, *119*, e2209630119. [CrossRef]
26. Jin, S.; Yang, W.; Zhang, L.; Sun, Y. Experimental study on gamma heating rate measurement based on differential calorimeter. *Ann. Nucl. Energy* **2024**, *207*, 110722. [CrossRef]
27. Hughes, L.; Kennett, T.; Prestwich, W. A study of the 55Mn(n, γ)56Mn reaction. *Nucl. Phys.* **1966**, *80*, 131–144. [CrossRef]
28. Vansola, V.; Mukherjee, S.; Naik, H.; Suryanarayana, S.V.; Ghosh, R.; Badwar, S.; Lawriniang, B.M.; Sheela, Y.S. Determination of55Mn(n, γ)56Mn reaction cross-section at the neutron energies of 1.12, 2.12, 3.12 and 4.12 MeV. *Radiochim. Acta* **2016**, *104*, 749–755. [CrossRef]
29. Blomqvist, J.; Olofsson, J.; Alvarez, A.M.; Bjerkén, C. Structure and Thermodynamical Properties of Zirconium Hydrides from First-Principle. In *Proceedings of the 15th International Conference on Environmental Degradation of Materials in Nuclear Power Systems—Water Reactors*; Springer International Publishing: Cham, Switzerland, 2011; pp. 671–681. [CrossRef]
30. King, D.; Knowles, A.; Bowden, D.; Wenman, M.; Capp, S.; Gorley, M.; Shimwell, J.; Packer, L.; Gilbert, M.; Harte, A. High temperature zirconium alloys for fusion energy. *J. Nucl. Mater.* **2022**, *559*, 153431. [CrossRef]
31. Forty, C.; Karditsas, P. Uses of zirconium alloys in fusion applications. *J. Nucl. Mater.* **2000**, *283–287*, 607–610. [CrossRef]
32. Morandi, A.; Pettinari, D.; Zucchetti, M. Activation analysis of a compact Tokamak using Deuterium–Helium3 fuel. *Fusion Eng. Des.* **2026**, *222*, 115491. [CrossRef]

Disclaimer/Publisher's Note: The statements, opinions and data contained in all publications are solely those of the individual author(s) and contributor(s) and not of MDPI and/or the editor(s). MDPI and/or the editor(s) disclaim responsibility for any injury to people or property resulting from any ideas, methods, instructions or products referred to in the content.